Band alignment switching and the interaction between neighboring silicon nanocrystals embedded in a SiC matrix

V. Kocevski, O. Eriksson, and J. Rusz
Department of Physics and Astronomy, Uppsala University, Box 516, S-751 20 Uppsala, Sweden
(Received 12 March 2015; published 27 April 2015)

We present results from density functional theory study of the electronic properties of silicon nanocrystals (Si NCs) embedded in a silicon carbide (SiC) matrix, considering different combinations of various NCs and host matrix sizes. We show that the NC and the host matrix form a type-II band alignment, with the states at the top of the valence band being in the Si NC and the states at the bottom of the conduction band in the host matrix. Moreover, this band alignment can be interchanged with introducing oxygen at the interface. This interchange in the band alignment has a rather weak influence on the absorption of the system. We demonstrate that the charge densities of some valence band states can overlap with the charge densities of the neighboring NCs. We also demonstrate that this leakage of states is significant when the distance between the neighboring NCs is less than ∼1.6 nm.

DOI: 10.1103/PhysRevB.91.165429 PACS number(s): 73.22.−f, 73.20.−r, 73.63.Bd, 78.67.Bf

I. INTRODUCTION

In the ongoing quest of producing the next generation solar cells, which will be more efficient, and at the same time cheaper, the focus has turned to the usage of silicon nanocrystals (NCs). The research is mainly directed in employing the unique effect exhibited by the silicon nanocrystals (Si NCs)—quantum confinement. Using this effect, the nanoparticle's band gap can be tailored according to the specific needs just by changing the size. To utilize this effect for making solar cells, where efficient charge extraction and transport is required [1], the silicon NCs must be embedded in a host matrix. However, the process of embedding the Si NCs may introduce defects and impurities, especially at the interface between the NC and the host matrix, which can facilitate recombination of the photoinduced excitons, substantially decreasing the efficiency of energy conversion of the solar cells [2]. Therefore, one way to lower the probability of charge recombination, is to spatially separate the electron and hole, by making a so-called type-II band alignment, where the valence band maximum (VBM) and conduction band minimum (CBM) are in different parts of the complex system.

The most commonly used host matrices, amorphous SiO_2, Al_2O_3, and Si_3N_4, form a type-I band alignment with the Si NCs [3–9], where both the VBM and CBM are in the NC. Thus, it is important to resort to finding new types of host matrices which have type-II band alignment with the Si NCs, and preferably with smaller band gaps that can allow increased tunneling of carriers in the complex system, hence increasing the conductivity [10]. For example, Wippermann *et al.*, based on density functional theory (DFT) calculation, have shown that Si NCs embedded in amorphous ZnS host matrix form type-II band alignment [11], where the VBM is in the host matrix and the CBM in the Si NC. However, for practical purposes a host matrix that can be cheaply and easily deposited, and on which Si NCs can be grown, is more desirable. One such complex system, consisting of Si NCs embedded in amorphous SiC, has been recently shown to exhibit promising properties for a third generation of photovoltaics [12–14].

In this paper we focus on the closely related system, considering Si NCs embedded in crystalline SiC. We employ DFT calculations, combined with classical molecular dynamics (MD) simulations, to study the electronic properties of this complex system. We consider three different sizes of NCs and three different sizes of the host matrix. These different models give us the opportunity to investigate the changes in the electronic properties of the systems with changes in the NC size and the distance between neighboring NCs. We show that due to underbonded atoms at the interface between the Si NC and the host matrix, there are impurity states in the region around the Fermi level, which can be eliminated by introducing hydrogen or oxygen at the interface. Furthermore, we observe a type-II band alignment, where the VBM is located in the Si NC and the CBM in the host matrix. Notably, we show that the band alignment can be interchanged by introducing oxygen at the interface, which slightly influences the absorption indices of the studied models. We also demonstrate that there is a possible leakage of some valence band (VB) states between the neighboring Si NCs. With increasing NC distance, the leakage is significantly decreasing, becoming almost absent when the distance between the NCs is more than ∼1.7 nm.

II. STRUCTURAL MODELS AND METHODOLOGY

For the purpose of our study we used crystalline SiC with zinc-blende structure as a host matrix, made of $6 \times 6 \times 6$, $7 \times 7 \times 7$, and $8 \times 8 \times 8$ unit cells of SiC, with lattice parameter of 4.36 Å. Depending on the size of the matrix, we embedded spherical Si NCs with three different diameters, 1.5 (87 Si atoms), 2.0 (191 Si atoms), and 2.5 (417 Si atoms) nm. In the $6 \times 6 \times 6$ matrix we embedded only the smallest NC, 1.5 nm; in the $7 \times 7 \times 7$ matrix we embedded the 1.5 and 2.0 nm NCs; and in the biggest matrix, we embedded NCs with all three considered sizes. Because our interest is also focused on the influence of the interface between the Si NCs and the host matrix, we modeled four different types of interfaces: matching (model A), distorted (model B), hydrogenated (model C), and oxygenated (model D).

The Si NCs in model A were made by replacing the C atoms with Si atoms within a given diameter (1.5, 2.0, or 2.5 nm)

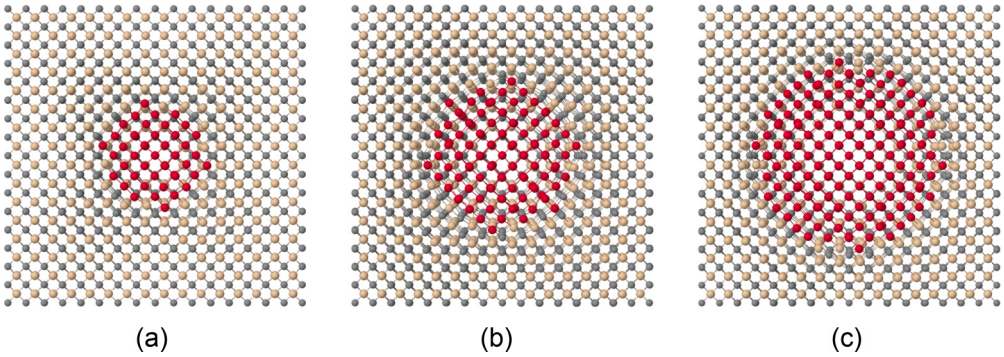

FIG. 1. (Color online) Ball and stick models of (a) 1.5 nm, (b) 2.0 nm, and (c) 2.5 nm Si NCs, embedded in $8 \times 8 \times 8$ SiC (model A). The Si atoms from the NCs are shown in red, and the Si and C atoms from the matrix are shown in tan and gray, respectively.

from the center of the SiC matrix. The lattice parameter of the Si NC was then scaled to match that of bulk Si, 5.43 Å, while the matrix lattice parameter was radially scaled to avoid overlapping between the NC and the matrix (see Fig. 1). The model B was made by removing a sphere from the matrix with the same diameter as the Si NC; afterwards a Si NC was inserted in the spherical hole made in the matrix. These two models represent a case of Si NCs grown from Si-rich SiC, where the former, model A, represents an ideal bonding situation between the NC and the matrix, and the latter a case where defects are introduced. The model C was made in a similar way as the model B, by inserting a Si NC in a hole in the matrix, with the same diameter as the NC. However, in the model C we first removed all nearest neighbors of the Si NC coming from the matrix, and later the Si and C atoms with less than four nearest neighbors were hydrogenated. The model D was made from model C, by replacing every pair of H atoms, closer than 1.1 Å, with an oxygen atom, i.e., inserting a bridged oxygen (–O–) between the Si NC and the SiC matrix. At the end there are 36, 36, and 84 oxygen atoms in the model D with 1.5, 2.0, and 2.5 nm NCs, respectively. The models C and D can be considered as representative of the case where previously synthesized Si NCs are being inserted in a SiC matrix. In an ideal case, the Si NCs would be fully hydrogenated, thus it is possible for hydrogen to be present at the interface of the NC and the matrix. Moreover, the Si NCs can be easily oxidized, which we simulate by inserting bridged oxygen between the NC and the matrix.

Models A and B were first relaxed using classical MD, using the LAMMPS code [15], employing the Erhart and Albe [16] parametrization of the SiC Thersoff pair potential. The relaxation was performed using the conjugate gradient algorithm, enforcing an energy and force convergence criterion of 10^{-10} eV and 10^{-14} eV/Å, respectively. During the relaxation the volume of the cell was allowed to relax, keeping the pressure of the system at 1 bar. Afterwards, the electronic properties of all four models were calculated using DFT as implemented in the pseudopotential package SIESTA [17], with local density approximation exchange-correlation potential. We used single-ζ polarized numerical atomic orbitals as a basis set for Si, C, and O, and double-ζ for H. The integration of the Brillouin zone was carried out only at the Γ point.

III. RESULTS AND DISCUSSION

The calculated density of states (DOS) are shown in Fig. 2. In the case of models C and D, there is a clearly distinguishable band gap in the DOS, which is increasing with decreasing NC size and lowering of the matrix size. Both of these observations are the consequence of the decreased concentration of the wider band gap material, the SiC, with the band gap also being influenced by the quantum confinement effect. However, in the DOS of models A and B the band gap is difficult to identify, because of the impurity levels in the region around the Fermi level. It is also interesting to notice that the states at the top of the VB are almost independent of the size of the SiC matrix (see left part in Fig. 2), indicating that these states are probably localized in the NC. On the other hand, the states at the bottom of the conduction band (CB) are influenced significantly more by the changes in the SiC matrix size, revealing an increased localization of the CB states in the matrix. Moreover, when the matrix size is kept constant and the NC size is changing, both VB and CB states around the gap are modified. These observations suggest a possible type-II band alignment, with the VBM being in the Si NC and the CBM being in the SiC matrix.

To have a better understanding where the impurity states are coming from, and to explicitly verify the type-II band alignment in the models, we calculated the projected density of states (PDOS) and the charge densities for each of the considered systems. Shown in Fig. 3 are the PDOS for the four different models, with 1.5 nm NC embedded in a $6 \times 6 \times 6$ matrix, divided into three regions of interest: (i) the Si NC core (Si atoms from the NCs that have four Si atoms as neighbors); the interface between the NC and the SiC matrix (the atoms from the NC and the matrix bonded with each other, or H or O atoms); and the SiC matrix (the atoms from the matrix that are not bonded to atoms from the NC, or H or O). Also shown in Fig. 3 are the projection of the charge densities on the x-y plane, calculated for 15 different energy intervals, between -1.5 and 1.5 eV.

It is evident that the impurity states in the region ± 0.7 eV around the Fermi level in models A and B, are mainly at the interface between the Si NC and the matrix. Considering the large lattice mismatch between Si and SiC, the states in this region can be assigned to the imperfections in the bonding between the Si NC and the matrix, and in the case of model B,

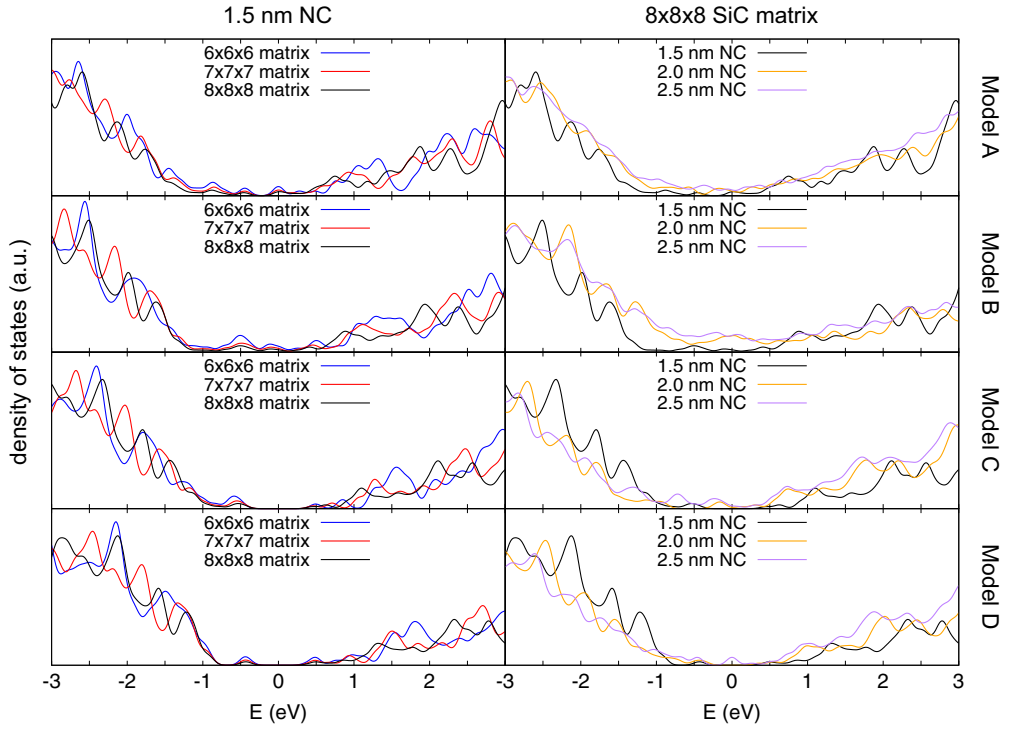

FIG. 2. (Color online) DOS of models A, B, C, and D, as a function of the size of the SiC matrix, for 1.5 nm NCs (left panel), and of the NC size for 8 × 8 × 8 matrix (right panel). The Fermi level is at 0 eV.

the presence of unsaturated bonds. From the charge densities in model A it is also noticeable that the states at the top of the VB are localized more in the Si NC, and the states at the bottom of the CB in the matrix, confirming a type-II band alignment. Although in model B there are many impurity states in the gap region, the slightly higher localization of the VB states in the Si NC, and the increased localization of the CB states in the matrix region, again shows type-II band alignment.

In model C there is a clearly defined band gap, where the states at the VBM are mainly localized in the Si NC and the CBM states in the matrix (note the charge densities in the 0.7–0.9 eV energy interval), showing a type-II band alignment, as in models A and B. Strikingly, in model D there is a reverse situation, where except for the impurity states coming from the interface, the VBM states are localized in the matrix, and the CBM states in the Si NC, still indicating type-II band alignment, but in reverse order. Keeping in mind that model D is made from model C by replacing some hydrogen atoms with oxygen, and comparing the PDOS of models C and D, it appears that the addition of oxygen at the interface causes the VBM of model C to move to the CBM of model D.

The shift of the VB states into the CB suggests that by introducing oxygen, or other elements with a higher number of valence electrons compared to Si, can modify the band alignment in systems with embedded Si NCs. A similar type-II band alignment as in model D is observed in Si NCs embedded in an amorphous ZnS matrix [11], where the Si NC is fully capped with sulfur atoms. However, with increasing Si NC size, the relative number of O atoms compared to the number of Si atoms of the NC is decreasing, and the contribution from the NC to the states at the top of the VB is growing. Eventually, in model D with 2.0 and 2.5 nm NCs the states at the VBM are predominantly localized in the NC, and the CBM states in the matrix. This can be clearly noticed in Fig. 4 from the changes in the position of the peak coming from the core states from the CBM to the VBM, when the size of the NC is increased.

This interchange in the band alignment, when oxygen is present, can give an explanation of the observed changes in the dark conductivity [18] of a system consisting of Si NCs embedded in a-SiC upon addition of oxygen [12]. In the system without oxygen, the states at the bottom of the CB are mainly in the host matrix, enabling the electrons to migrate freely, regardless of the size of the NCs. However, when oxygen is introduced, the band alignment is changed, and the CB states are predominantly in the core of the NCs, restricting the electron transport. With increasing the NC size, the NCs core states start to dominate in the VB, as seen from the PDOS in Fig. 4, restoring the band alignment as in the system without oxygen. This in turn allows the electrons to again move more freely, hence increasing the dark conductivity.

Besides the importance of the band alignment for photovoltaic applications, it is also necessary to gain a further knowledge of the absorption properties of the studied systems. Therefore, for the considered models we first calculated the imaginary part of the dielectric tensor, using the random phase approximation [19]. The Kramers-Krönig transformation was employed to obtain the real part of the dielectric tensor, from which the absorption indices were calculated. Shown in Fig. 5

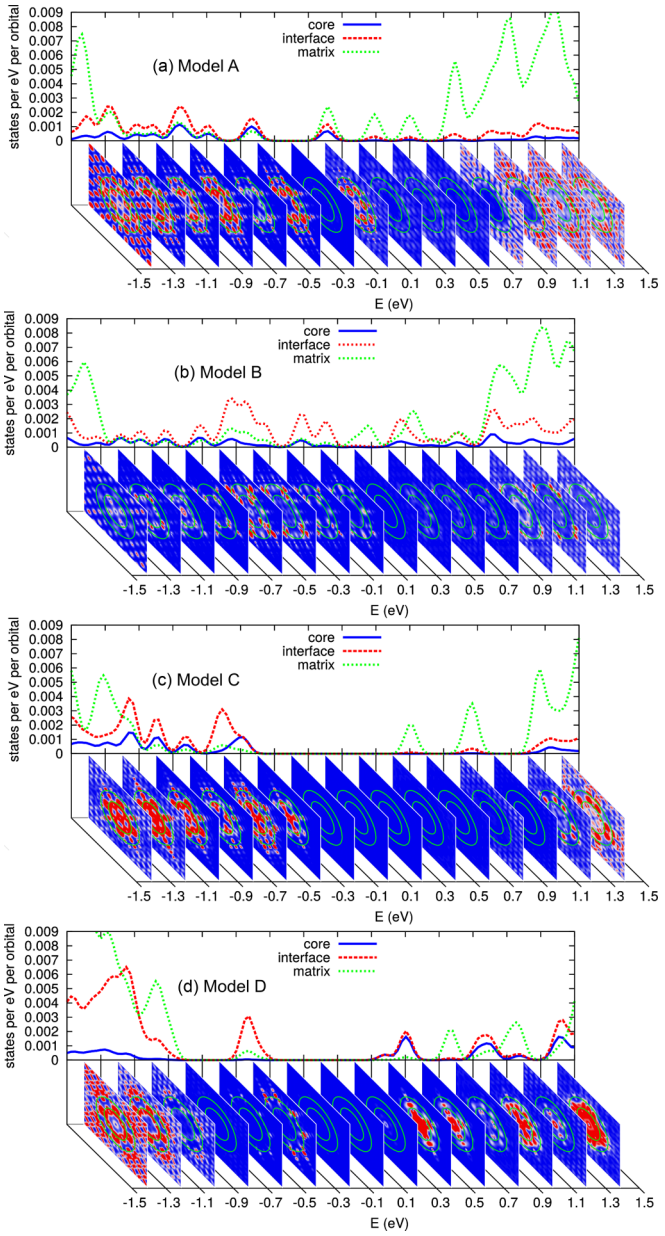

FIG. 3. (Color online) PDOS of (a) model A, (b) model B, (c) model C, and (d) model D, and the corresponding projections of the charge densities on the x-y plane. The PDOS of the core, interface, and matrix regions are shown in blue, red, and green, respectively.

are the calculated absorption indices for the models with $6 \times 6 \times 6$ and $7 \times 7 \times 7$ matrix size. It is interesting to note that the absorption indices of each of the smallest models [see Fig. 5(a)] appear to have a shape reminiscent of a linear combination of the absorption index of the Si NC and the SiC matrix, with some small extra peaks at lower energies. These small peaks are consequences of the impurity states around the Fermi level (see Fig. 3). Particularly, in model B this leads to a continuum of transitions at low excitation energies.

Interestingly, increasing the size of the matrix does not influence the position of the peaks in the absorption indices [see the same color lines in Figs. 5(a) and 5(b)]. In addition,

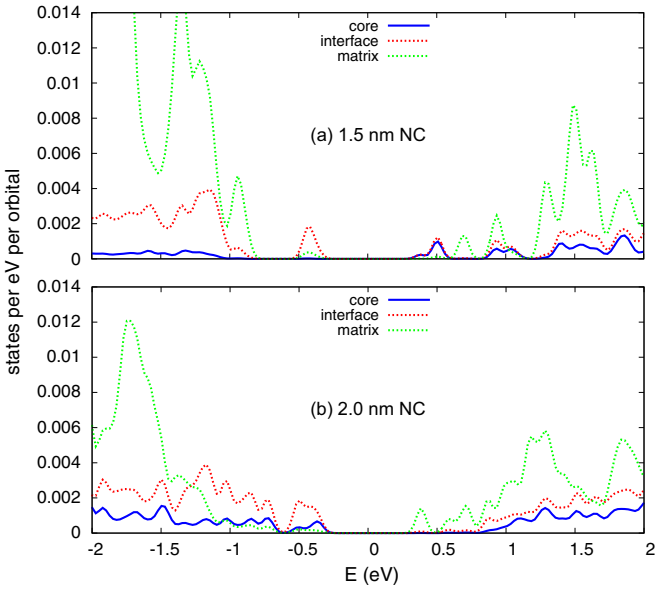

FIG. 4. (Color online) PDOS of model D with $7 \times 7 \times 7$ matrix with (a) 1.5 nm and (b) 2.0 nm Si NCs. The PDOS of the core, interface, and matrix regions are shown in blue, red, and green, respectively.

having the same size of the matrix, while increasing the NC size shifts the peak located at ∼5 eV to lower energies. In the models with opposite band alignment, e.g., models C and D with 1.5 nm NCs a similar behavior of the absorption indices is evident, regardless of the matrix size. Increasing the NC size to 2.0 nm in models C and D with $7 \times 7 \times 7$ matrix size, intensifies the similarity in the trend of the absorption indices. We remind one that the band alignment in models C and D with 2.0 nm NC is the same, and the same models with 1.5 nm NCs have interchanged band alignment. The slightly larger difference in the absorption indices of the models with 1.5 nm NCs indicates that the different band alignment has rather weak influence on the absorption. This suggests that the spatial separation of the charge carriers in the favorable bands, as discussed previously, would have the main influence on the efficiency of a solar cell made from these two materials. This discussion considers only the absorption in models with matrix size up to $7 \times 7 \times 7$. The calculations for the largest models were beyond our computational capabilities, but most importantly the qualitative trends seem to be possible to deduce already from the smaller systems.

Next we bring our attention to a charge density leakage of the states with predominant localization within the core. Notice in model A the states in the -0.5 to -0.3 eV energy interval, or in models B and C the states in the -0.7 to -0.5 eV energy interval. It is also interesting to notice that these states have increased contribution from the interface atoms. This suggests that the imperfections and impurity states at the interface might cause overlap of wave function between neighboring Si NCs. A potential leakage of the states can improve the efficiency of the solar cell by increasing the probability tunneling of the charge carriers.

The leakage of the states can be more easily understood by looking into a simple quantum mechanics example of

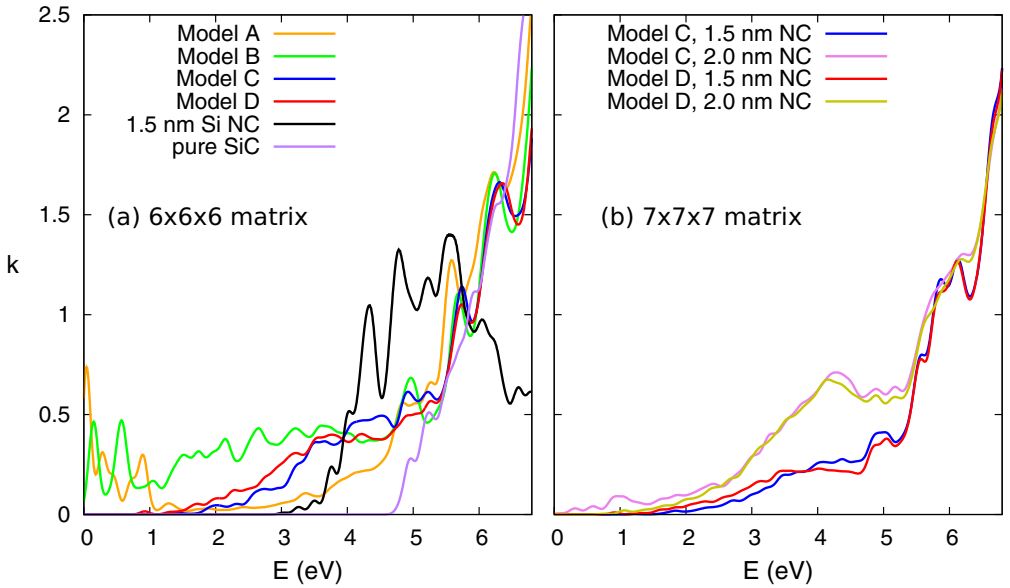

FIG. 5. (Color online) Absorption indices of Si NCs embedded in (a) $6 \times 6 \times 6$ SiC matrix and (b) $7 \times 7 \times 7$ SiC matrix, and different models. The absorption indices of models A, B, C, and D with 1.5 nm NCs are shown in orange, green, blue, and red, respectively. The absorption indices of models C and D with 2.0 nm NCs are shown in violet and yellow, respectively. The absorption indices of hydrogenated 1.5 nm Si NC and pure SiC are shown in black and purple, respectively.

an electron in a periodic potential well, $V(x)$, schematically represented in Fig. 6(a). The low potential area, V_0, represents the NC, and the host matrix is described by the potential barrier, with a height V_b. When the barrier width (in our models the NC-NC distance), d_b, is small enough, the tails of the electron wave function (WF) amplitude of the neighboring wells can overlap each other, indicating a leakage of state. Because the shape of the WF amplitude is dependent on the V_b, increasing d_b will only reduce the overlap between the neighboring WF amplitude. This can be viewed as a simplistic way to illustrate the leakage of states in models C and D, where all atoms at the interface are completely passivated.

Having a disordered interface or underbonded atoms at the interface can influence the confining potential, by increasing the probability of the charge density to spread in the area with higher potential. This is schematically shown in the right panel of Fig. 6(a) with a change in the shape of the potential barrier, causing an increased overlap between the tails of the neighboring electron WF amplitude. One should keep in mind that this is only a simple way to describe the notion of leakage of states, and a more exact description of the leakage of states in our models is best provided from accurate first-principles calculations, as will be discussed below.

To see how the wave functions' overlap depends on the distance between the NCs, we calculated the charge densities in the above-mentioned intervals, for the models with 1.5 nm NCs and three different sizes of the matrix, and for the $8 \times 8 \times 8$ model with three different sizes of NCs. The resulting isosurfaces of the charge densities, for two adjacent cells, are plotted as a projection on the x-y plane, using 10% of the maximum of each isosurface, and are shown in Fig. 6(b). Due to the spherical symmetry of the models, choosing other planes on which the charge densities are plotted would not change the qualitative picture.

With increasing the size of the matrix, i.e., increasing the distance between neighboring NCs [see Figs. 6(b) and 6(d)], the spatial distribution of the charge densities is rather unchanged, regardless of the model. However, the overlap between the charge densities of the neighboring cells is increasing with narrowing distance between the NCs. In the case of the models with the smallest NC distance, $\sim$1.2 nm, there is a noticeable leakage of the charge densities, with the charge density at the border of the two cells being $\sim$0.8% of the maximum charge density. The overlap is significantly reduced, when the distance between the NCs is $\sim$1.65 nm, $\sim$0.2% of the maximum, indicating a possible threshold at which the leakage between the charge densities dissipates. For larger distances, $\sim$2.1 nm, the leakage of the charge densities is almost absent, decreasing below 0.05% of the maximum.

Another way to investigate the influence of the distance between the NCs on the leakage of the charge densities, is to keep the matrix size constant and increase the NC size [see Fig. 6(c)]. In this case, the overlap between the charge densities is growing with growing NC size, i.e., decreasing NC distance, similarly to the previous example. It is also evident that the leakage between the states is largest for the biggest NCs, where significant overlap is observed, with more than 2% of the maximum charge density at the border of the two cells. When the distance between the NCs is $\sim$1.55 nm, the leakage is substantially decreased, with model A exhibiting larger overlap compared to model C, $\sim$0.45% and $\sim$0.15% from the maximum charge density for modes A and C, respectively. Comparing the leakage in the $8 \times 8 \times 8$ models with 2.0 nm NCs and $7 \times 7 \times 7$ models with 1.5 nm NCs, and keeping in mind the similar distance between the neighboring NCs, it is clear that the size of the NCs has rather weak effect on the leakage of the charge densities.

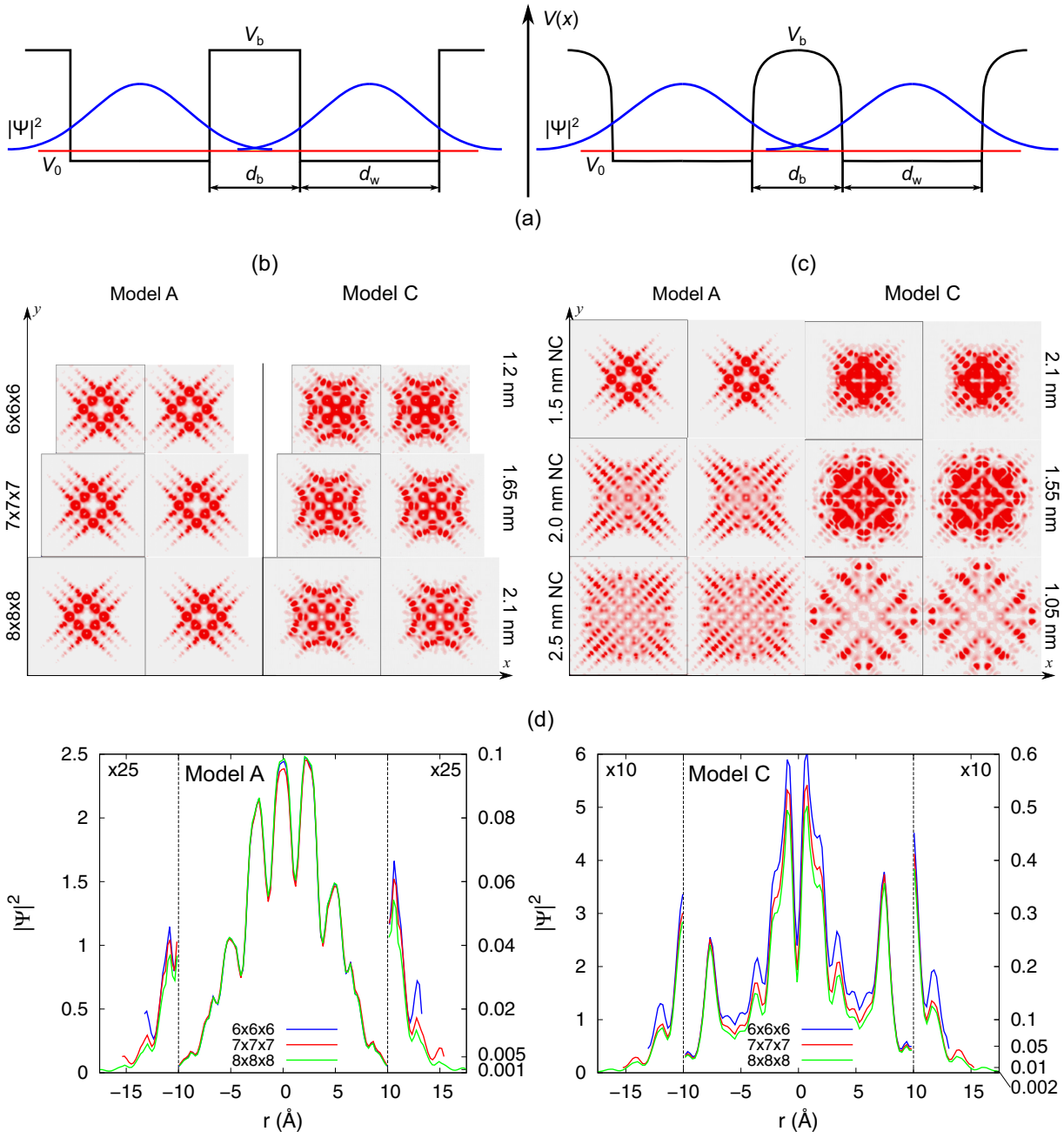

FIG. 6. (Color online) (a) Schematic representation of the WF amplitudes of electrons in a periodic potential well, with two different shapes of the potential barrier. Projections of the charge densities on the x-y plane, for two adjacent cells of models with (b) 1.5 nm NCs in different size matrix and (c) $8 \times 8 \times 8$ matrix with NCs with different size. The surface-to-surface distances between NCs in neighboring cells are given on the right side of each panel. The energy intervals, for which states the charge densities are calculated, of model A and model C are -0.5 to -0.3 eV and -0.7 to -0.5 eV, respectively. (d) Average charge densities in a series of {100} planes along the [100] direction, of models A (left part) and C (right part) with 1.5 nm NCs, corresponding to the same charge densities shown in (b).

IV. CONCLUSIONS

We show that there is a significant number of impurity states in the models with only Si NC and SiC matrix, arising from the distorted bond angle and/or underbonded atoms at the interface between the NC and the matrix. We demonstrate that the Si NC and SiC matrix form type-II band alignment, with the VBM being in the Si NC and the CBM in the host matrix. This band alignment can be reversed upon adding oxygen at the interface, showing a possible route how to tailor the band alignment between a Si NC and the host matrix. We have shown that the different band alignment has rather weak influence on the absorption indices of the studied models. Moreover, we demonstrate that there is a potential leakage of VB states between neighboring Si NCs, which can increase the efficiency of the solar cells. This leakage of the VB states is dependent on the distance between the Si NC, and is almost nonexistent when the distance is greater than $\sim$1.6 nm.

ACKNOWLEDGMENTS

This work was supported by the EU's 7th Framework Programme SNAPSUN. J.R. and O.E. acknowledge the support of Swedish Research Council. O.E. also acknowledges support from the Knut and Alice Wallenberg foundation and the European Research Council (Project No. 247062-ASD), as well as STANDUPP and eSSENCE.

[1] A. J. Nozik, Physica E **14**, 115 (2002).
[2] M. Green, *Third Generation Photovoltaics: Advanced Solar Energy Conversion*, Springer Series in Photonics (Springer, New York, 2006).
[3] K. Seino, F. Bechstedt, and P. Kroll, Phys. Rev. B **82**, 085320 (2010).
[4] C.-H. Cho, B.-H. Kim, S.-K. Kim, and S.-Ju. Park, Appl. Phys. Lett. **96**, 223110 (2010).
[5] G. Seguini, S. Schamm-Chardon, P. Pellegrino, and M. Perego, Appl. Phys. Lett. **99**, 082107 (2011).
[6] T. Li, F. Gygi, and G. Galli, Phys. Rev. Lett. **107**, 206805 (2011).
[7] M. Lei, J. H. Yum, S. K. Banerjee, G. Bersuker, and M. C. Downer, Phys. Status Solidi B **249**, 1160 (2012).
[8] G. Seguini, C. Castro, S. Schamm-Chardon, G. BenAssayag, P. Pellegrino, and M. Perego, Appl. Phys. Lett. **103**, 023103 (2013).
[9] V. V. Afanas'ev, Adv. Condens. Matter Phys. **2014**, 301302 (2014).
[10] G. J. Conibeer, C.-W. Jiang, D. König, S. Shrestha, T. Walsh, and M. A. Green, Thin Solid Films **516**, 6968 (2008).
[11] S. Wippermann, M. Vörös, A. Gali, F. Gygi, G. T. Zimanyi, and G. Galli, Phys. Rev. Lett. **112**, 106801 (2014).
[12] Y. Kurokawa, S. Yamada, S. Miyajima, A. Yamada, and M. Konagai, Curr. Appl. Phys. **10**, S435 (2010).
[13] J. Barbé, L. Xie, K. Leifer, P. Faucherand, C. Morin, D. Rapisarda, E. De Vito, K. Makasheva, B. Despax, and S. Perraud, Thin Solid Films **522**, 136 (2012).
[14] S. Perraud, E. Quesnel, S. Parola, J. Barbé, V. Muffato, P. Faucherand, C. Morin, K. Jarolimek, R. A. C. M. M. Van Swaaij, M. Zeman *et al.*, Phys. Status Solidi A **210**, 649 (2013).
[15] S. J. Plimpton, J. Comput. Phys. **117**, 1 (1995); http://lammps.sandia.gov/.
[16] P. Erhart and K. Albe, Phys. Rev. B **71**, 035211 (2005).
[17] P. Ordejón, E. Artacho, and J. M. Soler, Phys. Rev. B **53**, R10441 (1996); J. M. Soler, E. Artacho, J. D. Gale, A. García, J. Junquera, P. Ordejón, and D. Sánchez-Portal, J. Phys.: Condens. Matter **14**, 2745 (2002).
[18] Dark conductivity is a measure of the direct current flowing through a photosensitive sample under no incident illumination.
[19] S. L. Adler, Phys. Rev. **126**, 413 (1962).